Acta Cryst. (1973). A**29**, 537

High-Resolution Dark-Field Electron Microscopy. II. Short-range Order in Crystals

BY J. M. COWLEY

Department of Physics, Arizona State University, Tempe, Arizona 85281, *U.S.A.*

(*Received* 12 *December* 1972; *accepted* 9 *April* 1973)

The simple theory for the intensity distributions in high-resolution dark-field electron microscope images of thin specimens, derived from the phase-object approximation, is applied to discussion of images obtained from the diffuse scattering in electron diffraction patterns from crystals having short-range ordering of atoms on the lattice sites. It is shown that interpretation of the intensity distribution in terms of images of 'microdomains' is not usually justified. It is necessary to take into account the statistics of superposition of defects, possible dynamical diffraction effects and the fact that both positive and negative deviations from the average value of projected potential may give intensity maxima. Examples used to illustrate these points include a hypothetical case of a disordered CuAu crystal and some experimental observations of disordered $LiFeO_2$ showing a resolution of details on an atomic scale.

Introduction

One of the most attractive techniques for investigation of the nature of short-range ordering of atoms in crystalline solids appears to be the dark-field electron microscopy of thin crystals when the images are obtained from the diffuse scattering in the diffraction patterns due to the short-range ordering, the fundamental reflections due to the average structure being excluded. In recent years it has become clear that for many alloys and for many inorganic crystals the range over which correlation between atomic site occupancies extends may be 20 to 50 Å, as the apparent consequence of the existence of long-range interaction energy terms (see, for example, Cowley, 1971). The description of the short-range ordered state in terms of near-neighbor order parameters (or correlation coefficients) then becomes cumbersome. Instead, it is convenient to think in terms of the models of the system as built up of microdomains of an ordered structure separated by out-of-phase domain boundaries, such as are known to exist in regular array in an increasing number of ordered phases. It would seem to be well within the capabilities of present-day high-resolution electron microscopes to image such micro-domains and so 'prove' their existence and investigate the distribution of their shapes and sizes.

Dark-field images showing spots in the range of sizes to be expected for microdomains have been obtained, for example, by Ruedl, Delavignette & Amelinckx (1968) for Ni_4Mo, by Gaudig & Warlimont (1969) for Cu–Al alloys, by Warlimont & Thomas (1970) for α-Fe–Al, and by Watanabe & Fisher (1965) for $CuAu_3$. In general, the interpretation of such images has been made on the assumption that a white dot corresponds to a single microdomain oriented so that it gives rise to a diffuse diffraction spot which falls within the objective aperture.

In the first paper of this series (Cowley, 1973) we derived expressions for the intensity distributions in dark-field images of thin specimens and showed that a simple intuitive interpretation of a dark-field image as representing a density of scattering matter is often incorrect. In this paper we apply this theory specifically to the case of the imaging of diffuse scattering due to short-range order and attempt to establish a more realistic basis for the interpretation of the images.

2. The phase-object approximation

Most observations on short-range ordering are made using single crystals a few hundred Å thick. The range of validity of the phase-object approximation depends on the resolution involved, being 300–500 Å for 6Å resolution and about 100Å for 3Å resolution. Even though the crystal thickness may not come within these limits it may be assumed with some confidence that the phase-object approximation will give a reasonable indication of the observed contrast when applied to the imaging of relatively small domains within the crystal and hence the limitation of thickness may be less severe for cases we consider here. We assume then that for a plane incident wave, the wave leaving the crystal is

$$\psi(xy)=\exp\{-i\sigma\varphi(xy)\}, \qquad (1)$$

where $\sigma=\pi/\lambda E$, E is the accelerating voltage and $\varphi(xy)$ is the projection of the potential distribution in the beam direction.

As in the calculation of kinematical or dynamical diffraction intensities (Cowley, 1971) it is useful to write

$$\varphi(xy)=\bar{\varphi}(xy)+\Delta\varphi(xy) \qquad (2)$$

where $\bar{\varphi}$ is the periodic average potential projection which, kinematically, gives rise to the sharp 'fundamental' Bragg reflections, and $\Delta\varphi$ represents the derivations from this average, responsible, in kinematic scattering, for the short-range-order diffuse scattering.

In the phase-object approximation the sharp Bragg reflections are given by

$$\overline{\psi}(xy)=\overline{\exp\{-i\sigma(\varphi+\Delta\varphi)\}}$$
$$=\exp(-i\sigma\bar{\varphi})[1-i\sigma\overline{\Delta\varphi}-\frac{\sigma^2}{2!}\overline{\Delta\varphi^2}\ldots] \quad (3)$$

and since $\overline{\Delta\varphi}=0$ by definition, this is approximately equal to (for $\sigma\Delta\varphi$ not too large)

$$\psi(xy)\simeq\exp\{-i\sigma\bar{\varphi}\}\,.\,\exp\{-M\}\,, \quad (4)$$

where $M=\frac{1}{2}\sigma^2\overline{\Delta\varphi^2}$, and $\exp\{-M\}$ is an effective absorption factor representing the loss of energy from the Bragg spot to the diffuse background (Cowley & Pogany, 1968).

The diffuse-scattering amplitude is then given by the Fourier transform of

$$\psi_D(xy)=\exp\{-i\sigma\varphi\}-\overline{\psi}(xy)$$
$$=\exp\{-i\sigma\bar{\varphi}\}\,.\,[\exp\{-i\varphi\Delta\varphi\}-\exp\{-M\}]\,. \quad (5)$$

Under ideal dark-field imaging conditions, the sharp Bragg reflections would be completely excluded and the image would be obtained only from the diffuse scattering derived from (5). For the optimum defocus condition the phase factor, χ, due to defocus and spherical aberrations may be assumed to be zero over the objective aperture (Cowley, 1973). Then, apart from the limitations of resolution due to finite aperture size and ignoring the magnification factor, the image amplitude will be given by (5) and the image intensity by

$$I_D(xy)=|\exp\{-i\sigma\Delta\varphi\}-\exp\{-M\}|^2$$
$$=1+\exp\{-2M\}-2\exp\{-M\}\cos\sigma\Delta\varphi(xy)\,. \quad (6)$$

The form of this dependence on $(\sigma\Delta\varphi)$ is suggested in Fig. 1. For small deviations from the average projected potential, the intensity will be proportional to $[\Delta\varphi(xy)]^2$. This should be a good approximation for the short-range ordering of light atoms or of heavy atoms not differing greatly in atomic number. However for an alloy such Au–Cu where the deviation of the projected potential for each atom is equivalent to the projected potential of a moderately heavy atom, this approximation may fail for a microdomain of thickness of the order of 20 Å (*cf.* Cowley & Murray, 1968). However it seems unlikely that within the range of thicknesses for which the phase-object approximation is valid, the values of $\sigma\Delta\varphi$ will exceed that for the first of the damped oscillations of (6) or Fig. 1.

In general, dark-field images are obtained by use of an aperture of diameter less than the distance between the sharp Bragg reflections. Hence the lattice periodicity will not be resolved. Also the image intensity will depend on the position of the aperture with respect to the various diffuse maxima of the short-range-order diffuse scattering. In terms of the micro-domain picture, the contrast will be determined by the statistics of the overlapping of microdomains in the projection $\varphi(xy)$.

These points are best illustrated by examples.

3. A hypothetical case of disordered CuAu

We assume that a crystal of disordered CuAu of thickness 300 Å is made up of microdomains of the CuAuI structure of average dimension 20 Å separated by boundaries parallel to (100) planes. The unique c-axis direction of the CuAuI structure (for which the tetragonality is ignored) is assumed to vary at random between domains among the three equivalent orientations. The incident electron beam is assumed to be parallel to the [001] direction so that the diffraction pattern consists of strong sharp $2h, 2k, 0$ spots with diffuse maxima if h and k are not both even. The objective aperture is assumed to transmit only the 100 diffuse spot so that only those microdomains with c axis parallel to [100] will contribute to the image. Thus for an average of 15 microdomains in the crystal thickness, an average of five microdomains contributing to the 100 spot will be overlapped in the beam direction.

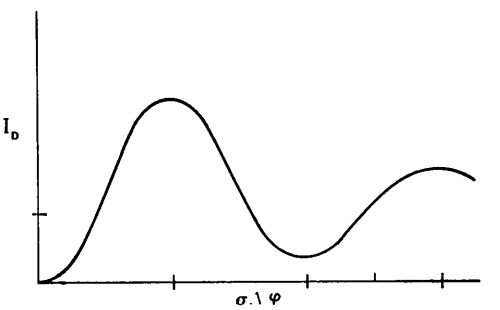

Fig. 1. The dependence of the intensity in a dark-field image on the deviation from the average potential in the phase-object approximation.

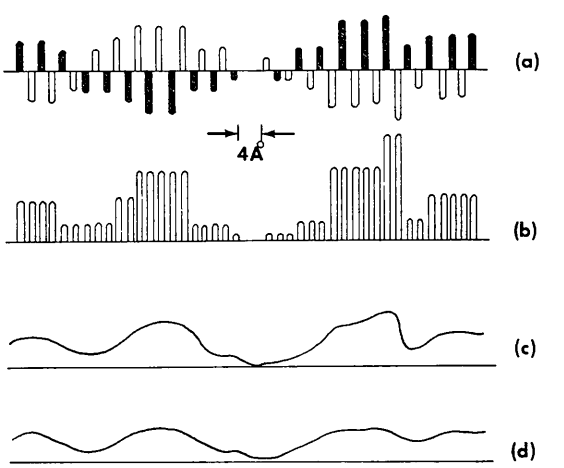

Fig. 2. (*a*) Deviations from the average projected potential for disordered CuAu. Alternate planes are made dark and light to emphasize changes of 'phase' of the deviations. (*b*) The square of the same function. (*c*) Dark-field image intensity produced with limited resolution: small-deviation approximation. (*d*) Dark-field image intensity when small deviation approximation fails.

For a single contributing domain, m atoms thick, the deviations from the average projected potential along a line parallel to the [100] direction will be alternately $\frac{1}{2}m(\varphi_{Au}-\varphi_{Cu})$ and $\frac{1}{2}m(\varphi_{Cu}-\varphi_{Au})$ as the beam passes through alternate Au and Cu planes. For an average of five microdomains overlapping at random the variation of $\sigma\Delta\varphi$ along such a line will be as suggested in Fig. 2(*a*). Positive peaks (excess Au) and negative peaks (excess Cu) will in general alternate but the heights will change as microdomains start or end at an average interval of 4 Å and the sequence of positive and negative peaks may be inverted as the number of 'in-phase' or 'out-of-phase' microdomains fluctuates.

If we make the simple small-deviation approximation to (6) the image intensity for ideal dark-field imaging is given by $(\sigma\Delta\varphi)^2$ as in Fig. 2(*b*). Then applying the resolution limitation due to the finite aperture we obtain the observed intensity distribution, Fig. 2(*c*).

If, on the other hand, we assume that the maximum values of $\sigma\Delta\varphi$ extend to the first maximum of the curve of Fig. 1, then the form of the observed intensity distribution will be more like Fig. 2(*d*) with the higher peaks suppressed.

We conclude that the intensity of white spots appearing in the dark-field image of such a disordered crystal will not in general give a direct indication of the individual microdomain dimensions or scattering power but will be determined by the statistics of overlap of contributing microdomains in projection and will vary non-linearly with the square of the deviation from the average projected potential.

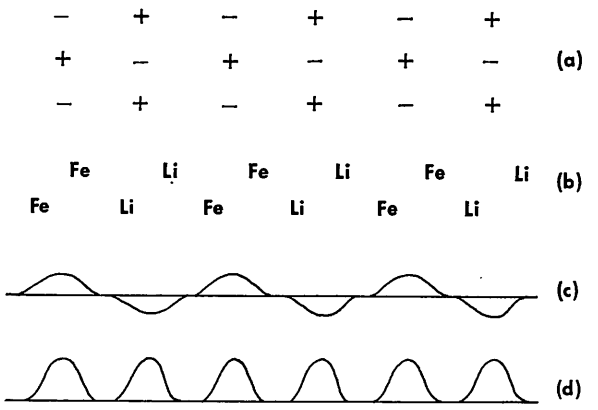

Fig. 4. (*a*) The form of the deviations from the average lattice of $LiFeO_2$ suggested by the diffraction patterns. The plus and minus signs indicate deviations in projected potential. (*b*) A possible configuration of Li and Fe ions giving these deviations. (*c*) The form of the deviations from average potential, spread by limited resolution. (*d*) The dark-field intensity distribution corresponding to (*c*).

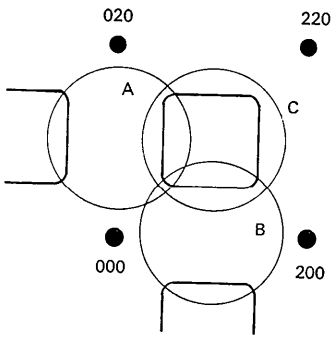

Fig. 6. Sketch of the diffraction pattern of Fig. 3 showing the approximation positions, *A*, *B* and *C* of the objective apertures used to obtain dark-field images.

4. Observations on disordered $LiFeO_2$

It has been shown by Brunel & de Bergevin (1969) that in the high-temperature α-phase of $LiFeO_2$ the Li and Fe ions are disordered on the cation sites of the NaCl-type lattice. Electron diffraction patterns such as Fig. 3 show a distribution of diffuse scattering (Allpress, 1971; O'Keefe, 1972) which may be considered as made up of planar sheets of diffuse scattering power perpendicular to the cube axes and occuring at odd half-multiples of the reciprocal-lattice axial translations.

This suggests that the short-range ordering takes the form of linear arrays of metal atoms parallel to the axis with positive and negative deviations in the projected potential alternating with a periodicity of $2a_0$, as suggested in Fig. 4(*a*). Since the planes of diffuse scattering have zero intensity where they intersect the axes, we postulate that each positive deviation point is surrounded by negative deviations of one-quarter strength at each of its nearest-neighbor positions.

The positive and negative deviation points may be taken to be pairs of iron and lithium atoms respectively, in the configuration suggested by Fig. 4(*b*) which occurs in the low-temperature ordered (γ or Q_1) phase (Brunel & de Bergevin, 1968). The curvature of the diffuse lines around their points of intersection and the enhancement of the intensity at these points which sometimes occurs may be explainable in terms of the form of the interactions of intersecting linear arrays.

The deviation from the average projected potential for one linear array is sketched in Fig. 4(*c*) and the resulting dark-field intensity distribution in Fig. 4(*d*). Thus one expects to see rows of white dots with a spacing of 4 Å, the unit-cell periodicity. Such rows of dots are visible in Fig. 5, obtained using a modified JEM-100B electron microscope (Iijima, 1971). This image was obtained with the aperture position indicated as *A* in Fig. 6, containing parts of two diffuse lines perpendicular to the [100] direction. The aperture position *B* gave similar rows of dots at right angles. However it cannot be assumed that these lines of dots are images of single defects.

The crystal giving the image of Fig. 5 was probably several hundred Å thick so that the contrast presumably arises from the superposition of the projections of several tens of the linear arrays giving either positive or negative peaks in $\sigma\Delta\varphi$ at 4 Å intervals. Furthermore,

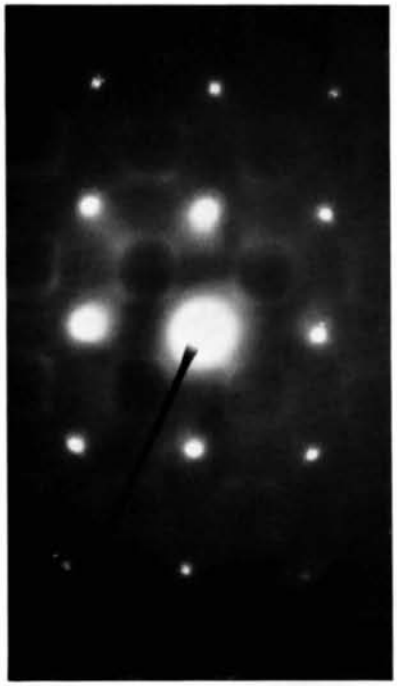

Fig. 3. Electron diffraction pattern of $LiFeO_2$ with incident beam parallel to cube axes, showing diffuse scattering.

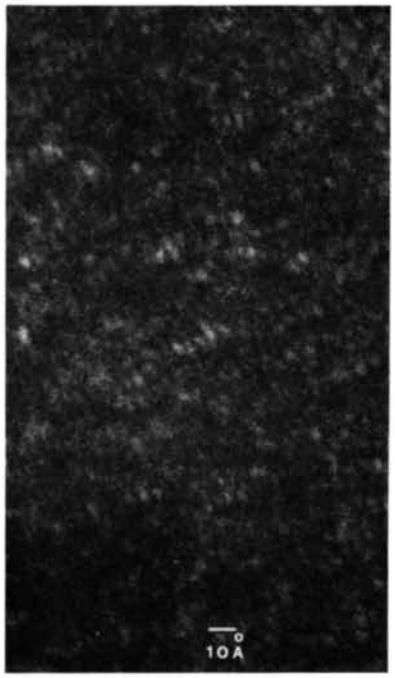

Fig. 5. Dark-field image of a thin $LiFeO_2$ crystal obtained from the diffuse scattering falling within the aperture in position *A* of Fig. 6.

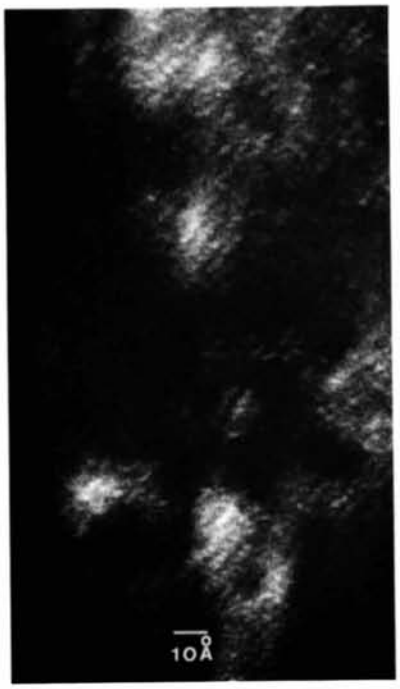

Fig. 7. Dark-field image of a thin $LiFeO_2$ crystal obtained from the diffuse scattering falling within the aperture in position *C* of Fig. 6.

[*To face p.* 540

the form of the image is strongly dependent on the objective-aperture position. For example Fig. 7, taken with an aperture near the position *C* of Fig. 6, shows lines of spots 4 Å apart but with a spot spacing of about 2·9 Å corresponding to the nearest-neighbor metal-atom separation.

5. Conclusions

Although the high-resolution dark-field electron microscope images which can now be obtained undoubtedly contain a great deal of information regarding short-range ordered crystals, it is clear that interpretation of this information in terms of microdomain models or particular forms of preferred atom correlations is not straightforward for the types of specimen and imaging conditions normally employed.

The use of very thin crystals (50 Å or less) would seem to offer the possibility of easier interpretation, but, apart from the experimental difficulties of obtaining such specimens, the question then arises as to whether the structures seen in such thin regions are representative of bulk structures.

For moderately thick crystals the phase-object approximation will cease to apply and the many complications of three-dimensional *n*-beam dynamical scattering of both the Bragg spots and the diffuse scattering will introduce complications which are difficult to appreciate (Cowley & Murray, 1968) and require excessive computing times for any but the most approximate calculations (Fischer, 1965; Doyle, 1969).

The combined use of electron diffraction patterns and electron microscope images appears to provide the best approach to studies of short-range ordering. Difficulties arise from the limitations of the usual selected-area electron diffraction technique in that the minimum area which can be used to obtain a diffraction pattern is of diameter 1μ or so for 100 keV electrons whereas the crystal thickness or orientation or other factors govering the image vary appreciably over distances of a few hundred Å. The development of scanning transmission electron microscope techniques may help to overcome this limitation (Cowley, 1970).

Our observation on $LiFeO_2$ serve to illustrate the difficulties involved in trying to derive more information from the image than is contained in the diffraction pattern. The nature of the interaction between linear arrays which presumably give rise to the curvatures of the diffuse lines in the diffraction pattern could not be deduced readily from the image, partly because of the superposition of many linear arrays in projection and partly because the distinction between positive peaks (iron atom concentrations) and negative peaks (lithium atom concentrations) in the projected potential was lost. This distinction would be retained in a bright-field image but the contrast due to the short-range ordering which we observed in bright-field images was low and, as in dark field images, the interpretation is confused by the superposition of a number of defects in projection.

This work was supported in part by the NSF Area Development Grant in Solid-State Science, No. GU 3169. The author is grateful for the valuable assistance of Mr John C. Wheatley who carried out the microscopy and diffraction studies on $LiFeO_2$.

References

ALLPRESS, J. G. (1971). *J. Mater. Sci.* **6**, 313–318.
BRUNEL, M. & DE BERGEVIN, F. (1968). *J. Phys. Chem. Solids*, **29**, 163–169.
BRUNEL, M. & DE BERGEVIN, F. (1969). *J. Phys. Chem. Solids*, **30**, 2011–2021.
COWLEY, J. M. (1970). *J. Appl. Cryst.* **3**, 49–59.
COWLEY, J. M. (1971). In *Advances in High-Temperature Chemistry*, Vol. 3, pp. 35–82. Edited by LEROY EYRING. New York and London: Academic Press.
COWLEY, J. M. (1973). *Acta Cryst.* A**29**, 529–536.
COWLEY, J. M. & MURRAY, R. J. (1968). *Acta Cryst.* A**24**, 329–336.
COWLEY, J. M. & POGANY, A. (1968). *Acta Cryst.* A**24**, 109–116.
DOYLE, P. J. (1969). *Acta Cryst.* A**25**, 569–577.
FISHER, P. M. J. (1965). *Proc. Int. Conf. Electron Diffraction and Nature in Defects in Crystals*, Australian Acad. Sci., Paper 1H-4.
GAUDIG, W. & WARLIMONT, H. (1969). *Z. Metallkol.* **60**, 488–498.
IIJIMA, S. (1971). *J. Appl. Phys.* **42**, 5891–5893.
O'KEEFE, M. (1972). M. Sc. Thesis, University of Melbourne.
RUEDL, E., DELAVIGNETTE, P. & AMELINCKX, S. (1968). In *Electron Microscopy*, 1968. pp. 311–312. Edited by D. S. BOCCIARELLI. Rome: Tipografia Poliglotta Vaticana.
WARLIMONT, H. & THOMAS, G. (1970). *Metal Sci. J.* **4**, 47–52.
WATANABE, D. & FISHER, P. M. J. (1965). *J. Phys. Soc. Japan*, **20**, 2170–2179.